

Pressure tuning the Jahn-Teller transition temperature in NaNiO_2

Liam A. V. Nagle-Cocco,^{*,†} Craig L. Bull,[‡] Christopher J. Ridley,[‡] and Siân E.
Dutton^{*,†}

[†]*Cavendish Laboratory, University of Cambridge, JJ Thomson Avenue, Cambridge, CB3
0HE, United Kingdom.*

[‡]*ISIS Neutron and Muon Facility, Rutherford Appleton Laboratory, Didcot, OX11 0QX,
United Kingdom.*

[¶]*School of Chemistry, University of Edinburgh, David Brewster Road, Edinburgh, EH9
3FJ, United Kingdom.*

E-mail: lavn2@cam.ac.uk; sed33@cam.ac.uk

Abstract

Abstract: NaNiO_2 is a layered material consisting of alternating layers of NaO_6 and Jahn-Teller-active NiO_6 edge-sharing octahedra. At ambient pressure it undergoes a broad phase transition from a monoclinic to rhombohedral structure between ~ 465 K and ~ 495 K, associated with the loss of long-range orbital ordering. In this work, we present the results of a neutron powder diffraction study on powdered NaNiO_2 as a function of pressure and temperature from ambient pressure to ~ 5 GPa between 290 K and 490 K. The 290 K and 460 K isothermal compressions remained in the monoclinic phase up to the maximum pressures studied, whereas the 490 K isotherm was mixed-phase throughout. The unit-cell volume was fitted to a 2nd-order Birch-Murnaghan equation of state, with $B = 113(1)$ GPa. We observe at 490 K that the fraction of Jahn-Teller-distorted phase increases with increasing pressure, from 67.8(6)% at 0.71(2) GPa

to 80.2(9)% at 4.20(6) GPa. Using this observation, in conjunction with neutron diffraction measurements at 490 K from 5.46(9) GPa to 0.342(13) GPa, we show that the Jahn-Teller transition temperature increases with pressure. Our results are used to present a structural pressure-temperature phase diagram for NaNiO_2 . To our knowledge, this is the first diffraction study of the effect of pressure on the Jahn-Teller transition temperature in materials with edge-sharing Jahn-Teller-distorted octahedra, and the first variable-pressure study on a JT-active edge-sharing nickelate.

1 Introduction

Many transition metal oxides exhibit a Jahn-Teller (JT) distortion due to degeneracy in the $3d$ orbitals, manifesting as an elongation or compression of the MO_6 (M =transition metal ion) octahedra, generally with associated orbital ordering. Previous studies on the effect of pressure on materials containing JT-active ions have found that pressure can entirely suppress the JT distortion and orbital ordering.^{1,2} It has also been observed that application of pressure reduces the magnitude of distortion in MO_6 octahedra.³⁻⁷

One well-studied material under pressure is LaMnO_3 (with JT active d^4 Mn^{3+} ions).^{2,3,8} At ambient pressure it adopts the perovskite structure with corner-sharing MnO_6 octahedra. An ordered JT distortion results in an orthorhombic symmetry. At $T > \sim 750$ K the JT distortion is suppressed, and there is an increase in symmetry first to a cubic phase with octahedral tilting, and then at higher temperatures to a rhombohedral phase.⁹ The temperature-driven suppression of the JT distortion coincides with a marked increase in electronic conductivity.¹⁰ On application of pressure at room temperature $P < 8$ GPa, the JT distortion is decreased through reduction of the long Mn-O bond lengths.³ At ~ 11 GPa a rhombohedral phase with no JT distortion co-exists with the distorted orthorhombic phase,² becoming single-phase at ~ 12 GPa. Similarly, the manganese (III) quadruple perovskite $\text{LaMn}_7\text{O}_{12}$, exhibits a complete suppression of the JT distortion at ~ 34 GPa.¹

There are several interesting studies on JT-distorted compounds with edge-sharing oc-

tahedra. Here we describe three different examples classes, all containing JT-active d^4 Mn^{3+} . Mn_3O_4 , a spinel containing both Mn^{3+} and Mn^{2+} , has been found to exhibit different pressure-dependence of JT-distorted octahedra depending on morphology; for instance, in single-crystal Mn_3O_4 the JT distortion survives to 60 GPa,¹¹ whereas there are observed transitions to JT-free phases at much lower pressures in powdered¹² and nanorod¹³ Mn_3O_4 . ZnMnO_2 , also with spinel-type structure but with Zn^{2+} on the Mn^{2+} of Mn_3O_4 , has been studied to very high pressure (~ 52 GPa),¹⁴ with a transition reported at ~ 23 GPa which has been alternately described as a transition from JT-elongation to a slight JT-compression¹⁴ or a spin-crossover transition resulting in an insulator \rightarrow metal transition.¹⁵ CuMnO_2 , with delafossite structure, has also had the pressure-dependence of its JT distortion studied.¹⁶ It exhibits a higher compressibility in the long Mn-O bond than the short Mn-O bond similar to LaMnO_3 ³ and other materials^{4,5} up to around around ~ 10 GPa; above this pressure there is an isostructural phase transition associated with a collapse in the interlayer (c -axis) and an increase in the volume of the Mn^{3+}O_6 JT-distorted octahedra.

Nickelates containing JT-active d^7 Ni^{3+} are far less studied than the manganates under pressure. This may be partly because many materials containing d^7 Ni^{3+} octahedra do not exhibit a co-operative JT distortion, where the JT distortion is long-range ordered. NdNiO_3 , which has been subject to a variable-pressure structural study,¹⁷ is not considered to contain a JT distortion,^{18–20} as is the case for most Ni-containing perovskites.²¹ Similarly, AgNiO_2 is widely accepted to not contain any kind of JT distortion.^{22,23} LiNiO_2 is an interesting case as it does not display long-range magnetic or orbital ordering, likely due to Li/Ni site mixing; some experimental results have been interpreted as evidence for a non-cooperative JT distortion,^{24,25} although this is debated.^{26–28} Similarly various nickel-containing perovskites²⁹ are subject to discussion regarding whether there exists any kind of JT distortion.

NaNiO_2 is a layered d^7 nickelate. The presence of the JT distortion in NaNiO_2 is not subject to debate,^{28,30,31} even amongst proponents of alternative theories for degeneracy-breaking in LiNiO_2 .²⁸ NaNiO_2 is therefore an ideal choice for studying the effect of pressure

on the JT distortion in a material which is both a nickelate and has edge-sharing octahedra. The room-temperature phase of NaNiO_2 is a semiconductor, based on its black colour and by analogy with LiNiO_2 ,³² but we do not know of any measurement of the conductivity properties of the high-temperature phase. NaNiO_2 is of interest because of its magnetic ground state, consisting at ambient pressure of intra-layer ferromagnetism and inter-layer anti-ferromagnetism.^{33–35} It has also been studied in recent years because $A\text{NiO}_2$ ($A =$ alkali metal) is the template compound for Ni-rich alkali metal-transition metal oxides within the field of batteries.^{36,37}

NaNiO_2 has an ordered JT distortion at room temperature due to degeneracy in e_g orbitals in low-spin Ni^{3+} . It exhibits a first-order phase transition between 465 K and 495 K to an undistorted phase. The crystal structures are shown in Figure 1. The monoclinic ($C2/m$) JT-distorted phase consists of alternating layers of edge-sharing NiO_6 and NaO_6 octahedra. Both the NiO_6 and NaO_6 octahedra exhibit angular and bond-length distortions from geometrically regular octahedra. Ni, Na, and O ions occupy the $2a(0,0,0)$, $2d(0, \frac{1}{2}, \frac{1}{2})$, and $4i(x,0,z)$ Wyckoff sites respectively. The rhombohedral ($R\bar{3}m$) phase consists of the same arrangement of alternating NiO_6 and NaO_6 layers of edge-sharing octahedra, with octahedra bound within layers by O_4 tetrahedra. In this phase, Ni, Na, and O ions occupy the $3b(0,0, \frac{1}{2})$, $3a(0,0,0)$, and $6c(0,0,z)$ Wyckoff sites respectively. The unit cell remains centrosymmetric, with the change in symmetry due solely to the repression of the JT distortion and the resulting non-variable r_{M-O} bond lengths.

In this work, we present a structural study of NaNiO_2 as a function of temperature between 290 K and 500 K, and pressure up to 5.46(9) GPa. We demonstrate using the 490 K isotherm that the JT transition temperature increases between 2 GPa and 4.2 GPa, increasing more rapidly with pressure at higher pressures, while the degree of distortion decreases over this pressure range.

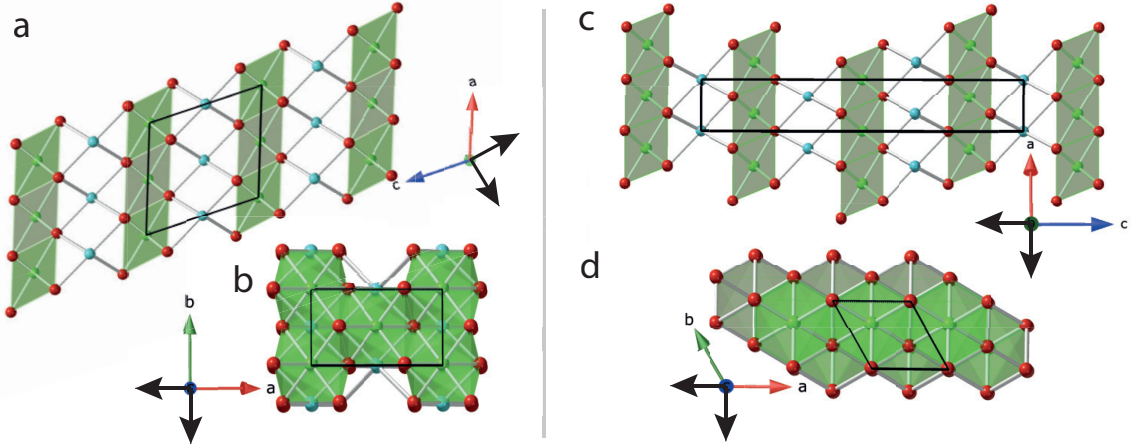


Figure 1: (a) and (b) show the monoclinic, Jahn-Teller distorted NaNiO_2 phase along the b -axis and c -axis respectively. (c) and (d) show the rhombohedral, JT-inactive NaNiO_2 phase along the b and c axes respectively. Ni^{3+} cations are shown in green, O^{2-} anions in red, and Na^+ cations in cyan. Na^+ ions and octahedra are hidden in (b) and (d). The solid black quadrilaterals denote the unit cell. The black arrows represent the directions of principal axes of compression projected into the (a,c) ac -plane and (b,d) ab -plane.

2 Methods

Sample preparation and characterisation. Samples were prepared by solid state synthesis. Na_2O_2 (Alfa Aesar; 95%) and NiO (Alfa Aesar; 99.995%) were mixed and pelletised in a 1.05:1 molar ratio of Na:Ni, with excess Na to account for Na-loss during heating. Sample was heated to 973K for 70 hrs in a tube furnace under constant flow of O_2 . To prevent reaction with moisture, the sample was stored and handled in an inert Ar-atmosphere. X-Ray Diffraction (XRD) data were obtained using a Bruker D8 Discover powder ($\text{Cu K}\alpha_{1,2}$, $\lambda = 1.541 \text{ \AA}$) diffractometer. A Mira3 TESCAN Scanning Electron Microscopy was used to obtain SEM images of the morphology of NaNiO_2 , with an accelerating electron voltage of 3 kV (for SEM images, see SI).

Ambient-pressure neutron diffraction. Ambient-pressure neutron diffraction was performed using the NOMAD instrument³⁸ at the Spallation Neutron Source, Oak Ridge National Laboratory, USA. NaNiO_2 was sealed in a glass ampoule for the measurements. Heating was performed using a furnace. The sample was measured during heating at 293 K, 450 K, 500 K, and after cooling at 316 K.

Variable-pressure neutron diffraction. Variable-temperature and -pressure neutron diffraction studies were performed at the PEARL instrument³⁹ ($2\theta = 90^\circ$), ISIS Neutron and Muon Source, UK, using a V3 Paris-Edinburgh press. The sample was measured between 0.107(8) GPa and 4.24(5) GPa at 290 K, 0.130(10) GPa and 5.29(8) GPa at 460 K, and 0.254(17) GPa and 4.20(6) GPa at 490 K. NaNiO₂ was packed into a encapsulated null scattering TiZr gasket which was loaded in a zirconia-toughened alumina toroidal profile anvil, with a lead pellet for pressure calibration.⁴⁰ Anhydrous deuterated methanol:ethanol (4:1 by volume) was used as a pressure transmitting medium for the ambient temperature isothermal compression experiment. Preliminary measurements indicated that NaNiO₂ reacted with the methanol:ethanol solution at higher temperatures [SI Figure S2], and so a 1:1 ratio by volume of FC77:FC84 fluorinert (purchased from 3M) was used for the 460 K and 490 K isotherms. The data were processed and corrected using Mantid.⁴¹

Diffraction Analysis. Diffraction data were analysed using the software package TOPAS 5,⁴² utilising Pawley fitting⁴³ and Rietveld refinement.⁴⁴ For NaNiO₂, preliminary analysis of NOMAD data indicated Na occupancy was 1 within error, hence site occupancy of all sites during all further refinement was fixed at 1. Thermal B_{eq} parameters were allowed to refine but constrained to be positive and not exceed a value of 5 \AA^2 . All atomic positions were refined within symmetry constraints. The background was fitted by a Chebyshev polynomial (order 6 for PEARL data, order 11 for NOMAD data, order 19 for XRD data). For XRD data, a TCHZ peak-shape was used.⁴⁵ Peak-shapes used for neutron data are discussed in SI Section II. For PEARL only the 90° detection bank was used, but for NOMAD a combined refinement was performed using banks 2-5 ($2\theta = 31^\circ, 67^\circ, 122^\circ, 154^\circ$ respectively).

3 Results

3.1 Ambient-pressure structural properties.

Powder X-ray diffraction of the as-synthesised NaNiO_2 indicated the formation of a phase-pure product. SEM on the material indicates the sample is polycrystalline with particulates between 0.2 μm and 5 μm in diameter [SI Figure S13]. Rietveld refinement using the reported monoclinic $C2/m$ space group [SI Figure S1; Table S1] yielded lattice parameters consistent with prior reports.^{30,46}

The reported monoclinic \Rightarrow rhombohedral phase transition in NaNiO_2 was investigated using neutron powder diffraction at ambient pressure on the NOMAD instrument. Rietveld refinement [Figure 2] shows the phase transition occurs between 450 K and 500 K, and is reversible on cooling. The lattice parameters [SI Table S2] all exhibit positive thermal expansion, and are consistent with previous measurements.^{30,31}

In the monoclinic structure the NiO_6 octahedra exhibit a cooperative JT distortion with 2 longer Ni-O bonds, whereas in the high-temperature rhombohedral phase all six Ni-O bonds are equivalent [Figure 1]. The degree of bond length distortion within individual NaO_6 and NiO_6 octahedra can be evaluated using a number of distortion metrics, calculated using TOPAS 5.⁴² Here we consider the effective coordination number⁴⁷ and the bond length distortion indices,⁴⁸ which measure distortion in octahedra by quantifying the difference from the average value of the distances between the central cation and the coordinated oxygen anions. The general form of effective coordination, ECoN, and bond length distortion index, D , is given in the SI. The equations as applicable to monoclinic NaNiO_2 are:

$$\text{ECoN} = 4 \exp \left[1 - \left(\frac{l_{\text{short}}}{l'_{\text{av}}} \right)^6 \right] + 2 \exp \left[1 - \left(\frac{l_{\text{long}}}{l'_{\text{av}}} \right)^6 \right], \quad (1)$$

where l'_{av} is a modified average bond length defined in SI, and;

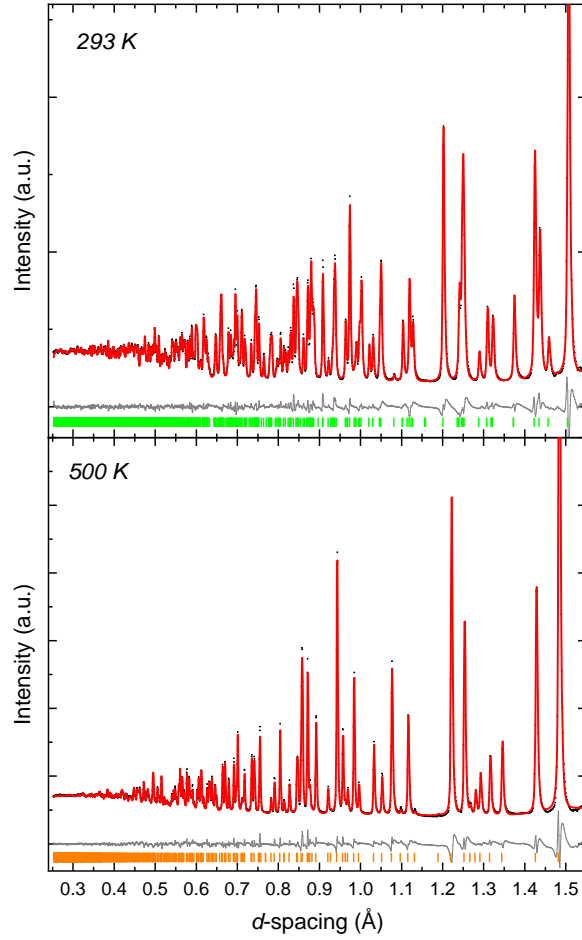


Figure 2: Rietveld refinements for the ambient-pressure, variable-temperature neutron diffraction measurements of NaNiO_2 on bank 5 of NOMAD ($2\theta = 154^\circ$) at 293 K (top) and 500 K (bottom). Black dots: measured data; red line: calculated diffraction pattern from Rietveld refinement; grey line: $Y_{\text{obs}} - Y_{\text{calc}}$. Green and orange tick marks show expected reflections for the monoclinic and rhombohedral phase respectively.

$$D = \frac{1}{3} \frac{l_{\text{long}} - l_{\text{av}}}{l_{\text{av}}} + \frac{2}{3} \frac{l_{\text{av}} - l_{\text{short}}}{l_{\text{av}}} \quad (2)$$

where l_{av} is the average bond length, and l_{long} and l_{short} are the long and short bonds respectively.

In the rhombohedral structure the effective coordination number and bond length distortion index of both the NiO_6 and NaO_6 octahedra are constrained by symmetry to values of 6 and 0 respectively. In the monoclinic structure, departure from these values indicates bond length disproportionation and is primarily attributable to the JT distortion. These changes are significantly larger for the JT-active NiO_6 octahedra than the NaO_6 octahedra. Throughout the measurement, the bond length distortion index {effective coordination} of NaO_6 octahedra remains very near its high-symmetry value of 0{6}, for example at 293 K the value of bond length distortion index {effective coordination} in NaO_6 octahedra is 0.00581(11){5.99232(19)}, compared with 0.05463(14){5.309(3)} in the NiO_6 octahedra. This is indicative of much greater distortion in bond lengths for NiO_6 octahedra, consistent with the JT distortion. The values of bond length distortion index are on the same order of magnitude as recent studies on JT-distorted Mn^{3+}O_6 -containing compounds.^{16,49}

Inconsistency in bond length is not the only distortion of the octahedra from regular octahedra. A regular octahedron would have bond angles $\theta_{\text{O}-M-\text{O}} = 90^\circ$ for nearest-neighbour O anions. However, in both the JT-active monoclinic phase and the JT-inactive rhombohedral phase there is variance from this ideal bond angle. Non-nearest-neighbour oxygen anions are constrained to have 180° bond angles via the central cation, and so the 12 bond angles in an octahedron are each paired with another O-M-O bond, with the paired bond angles sharing one oxygen in common and with their non-shared oxygen anions occurring along a straight line through the central cation (for a visual representation, see SI Figure S14). We define these bond angles as $\theta_{\text{O}-M-\text{O}} = 90^\circ \pm \Delta$, where the two angles in a pair have opposite sign preceding the Δ . Δ can also be thought of as a measure of the extent of angular distortion. In the rhombohedral structure, there is only one value of Δ for each type of octahedron,

with half the O-*M*-O bond angles being $90^\circ + \Delta$ and the other half being $90^\circ - \Delta$. In the monoclinic unit cell where octahedra have two long *M*-O (*M*=Na,Ni) bonds and four short *M*-O bonds, there are four nearest-neighbour bond angles between short and short bonds and eight nearest-neighbour bond angles between short and long bonds. We therefore must define two values of Δ for the bond angles in the monoclinic phase, $\Delta_{\text{short-short}}$ and $\Delta_{\text{long-short}}$, respectively. Table 1 shows these values of Δ at each temperature. It is clear that NaO_6 octahedra exhibit far higher bond angle distortion than NiO_6 octahedra, in contrast to the bond length distortion which is greater for NiO_6 octahedra. This is not unexpected, given that crystal field effects will result in much greater stability for open-shell d^7 Ni^{3+} in an octahedral configuration, minimising bond angle variance, whereas this won't be a factor for closed-shell Na^+ cations.

Table 1: This table shows the value of Δ for bond angles O-*M*-O (*M*=Na, Ni) which take the value $90^\circ \pm \Delta$, as a function of temperature. For definitions, check the main text. The arrow next to the temperature indicates whether the data were collected on warming or cooling of the sample.

Phase	T (K)	NiO_6 ($^\circ$)		NaO_6 ($^\circ$)	
		$\Delta_{\text{short-short}}^{\text{Ni}}$	$\Delta_{\text{long-short}}^{\text{Ni}}$	$\Delta_{\text{short-short}}^{\text{Na}}$	$\Delta_{\text{long-short}}^{\text{Na}}$
<i>C2/m</i>	293 (-)	6.134(17)	5.456(19)	14.494(12)	9.708(14)
<i>C2/m</i>	450 (\uparrow)	6.163(19)	5.50(2)	14.564(14)	9.844(16)
<i>R3m</i>	500 (\uparrow)	6.135(15)		11.777(13)	
<i>C2/m</i>	316 (\downarrow)	6.121(18)	5.46(2)	14.505(13)	9.731(15)

3.2 Variable-pressure neutron diffraction.

The effect of pressure on the JT distortion in NaNiO_2 was explored at 290 K, 460 K, and 490 K, with an example Rietveld refinement shown in Figure 3 and data shown in Figures 4-8. Over the entire pressure and temperature range studied NaNiO_2 could be described using the previously-reported ambient pressure crystal structures. Diffraction data also included contributions from alumina and zirconia in the sample environment and the lead used to determined the applied pressure - these are also included in the structural refinements.

In addition, at higher temperatures (460 K and 490 K) and pressures additional peaks attributed to crystallisation of the fluorinert pressure media [SI Figure S3] are observed in the measurements.

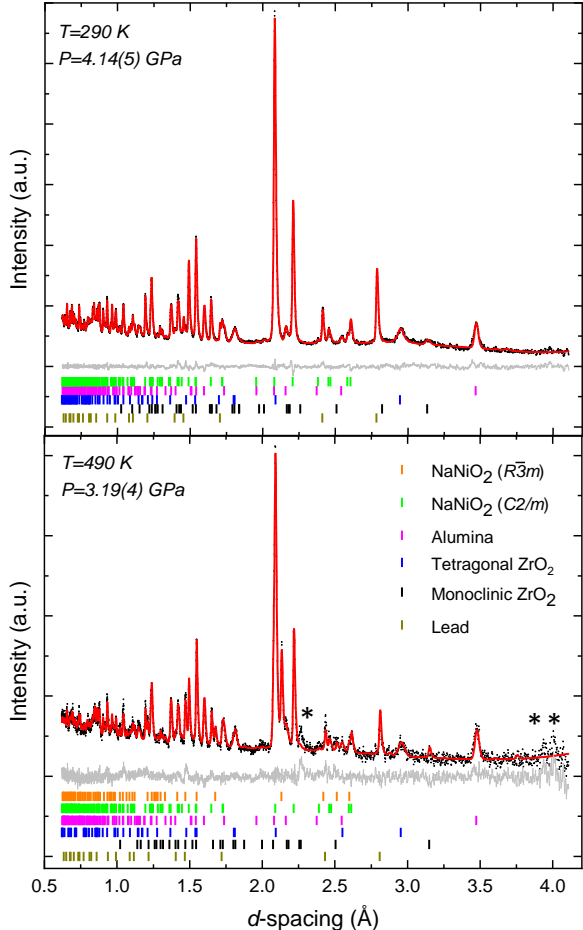


Figure 3: Rietveld refinements for the variable-pressure neutron diffraction data of NaNiO_2 . Top: a representative plot with monoclinic NaNiO_2 only; bottom: a representative plot with both monoclinic and rhombohedral NaNiO_2 . Black dots: measured data; red line: calculated diffraction pattern from Rietveld refinement; grey line: $Y_{\text{obs}} - Y_{\text{calc}}$. Unfitted peaks are marked with an asterisk and arise from crystalline fluorinert [SI Figure S3].

Rietveld analysis, Figure 3, shows that NaNiO_2 remained in the monoclinic phase at 290 K (up to 4.24(5) GPa) and 460 K (up to 5.29(8) GPa). However, the measurements at 490 K capture NaNiO_2 midway through its transition from JT-distorted $C2/m$ monoclinic to JT-inactive $R\bar{3}m$ rhombohedral, and throughout this isotherm the NaNiO_2 is mixed-phase.

The lattice parameters [Figure 4] show the expected variation with temperature and

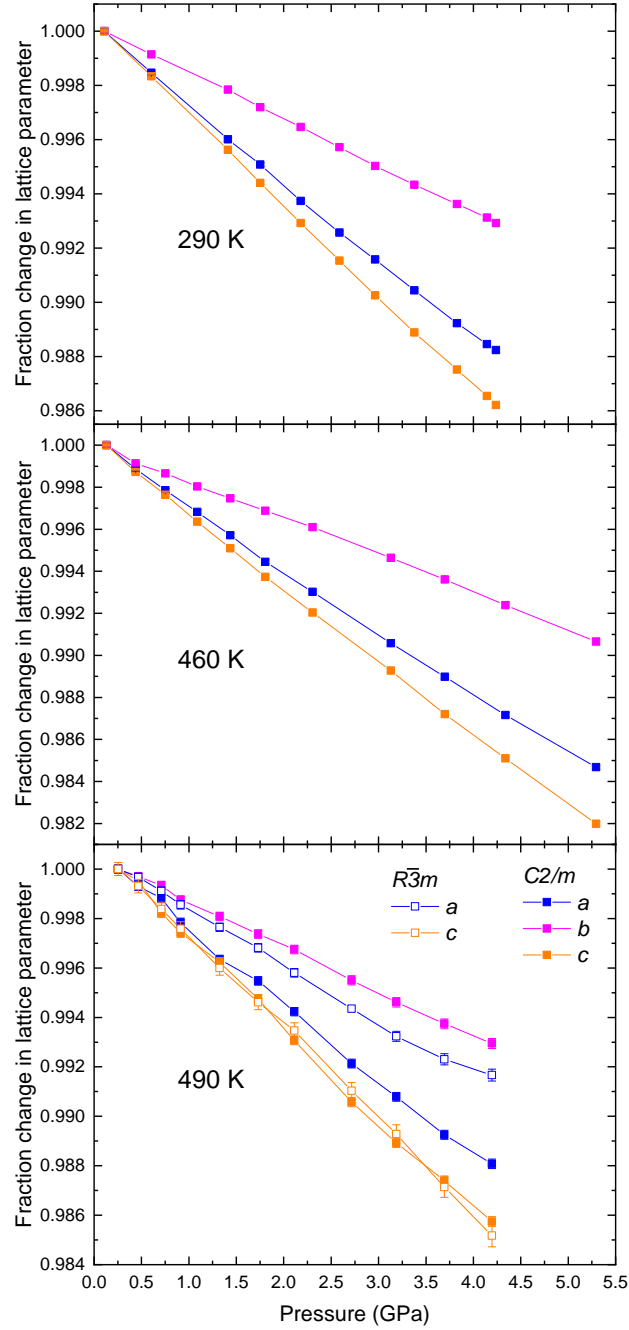


Figure 4: Fractional contraction of lattice parameters obtained by Rietveld refinement⁴⁴ as a function of temperature and pressure for the monoclinic $C2/m$ and rhombohedral $R\bar{3}m$ phases of NaNiO₂. Error bars are shown for all plots; where they are not visible it is because the error is smaller than the data point. Lines are a guide for the eye.

pressure. The rhombohedral and monoclinic phases have similar compressibility, and in both NaNiO_2 is considerably more compressible in the inter-layer direction (c -axis) than the intra-layer (ab -) plane. With reference to Figure 1, we note that compression within the plane results in changes to the highly ionic $\text{Na}^+\text{-Na}^+$ interactions and the less ionic, but still repulsive $\text{Ni}^{3+}\text{-Ni}^{3+}$ interactions, whereas compression in the inter-layer direction will compress the $\text{Ni}^{3+}\text{-O}^{2-}$ and $\text{Na}^+\text{-O}^{2-}$ bonds which are softer due to the nearest-neighbour interaction lacking a Coulomb repulsive force. This higher compressibility in the inter-layer direction is consistent with that seen in another material with alternating layers of edge-sharing octahedra, the honeycomb iridate Na_2IrO_3 .^{50,51}

Within the plane, in monoclinic NaNiO_2 , the b -axis is less compressible than the a -axis. A reason for this might be that $\text{Na}^+\text{-Na}^+$ and $\text{Ni}^{3+}\text{-Ni}^{3+}$ interactions are parallel to the direction of compression for the b -axis, maximising the increase in Coulomb repulsion with decreasing lattice parameter due to compression, whereas there are no $\text{Na}^+\text{-Na}^+/\text{Ni}^{3+}\text{-Ni}^{3+}$ interactions with components only along the a -axis. Another contribution may be that the $\text{Na}^+\text{-Na}^+$ and $\text{Ni}^{3+}\text{-Ni}^{3+}$ ionic distances parallel to the b axis are considerably shorter than the distances which can be projected onto the a -axis ($\sim 2.85 \text{ \AA}$ and $\sim 3.02 \text{ \AA}$ respectively at 290 K and 0.107(8) GPa).

Table 2: Parameters determined from the 2nd-order Birch-Murnaghan Equation of State, obtained using PASCAL⁵² [SI Section V, Table S12].

Structure	Temperature	$V_0 (\text{\AA}^3)$	B_0 (GPa)
$R\bar{3}m$	490 K	119.83(2)	113(1)
$C2/m$	490 K	79.900(16)	110(1)
	460 K	79.798(9)	113.5(6)
	290 K	79.258(7)	119.6(5)

PASCAL⁵² was used to obtain the bulk modulus for each isotherm, using a 2nd-order Birch-Murnaghan equation of state.⁵³ A plot of the unit cell volume obtained by Rietveld refinement, as a function of pressure, with a fit of this equation of state, is shown in Figure 5 and tabulated in Table 2. For the monoclinic phase, $\frac{dV_0}{dT} > 0$ which is consistent with a

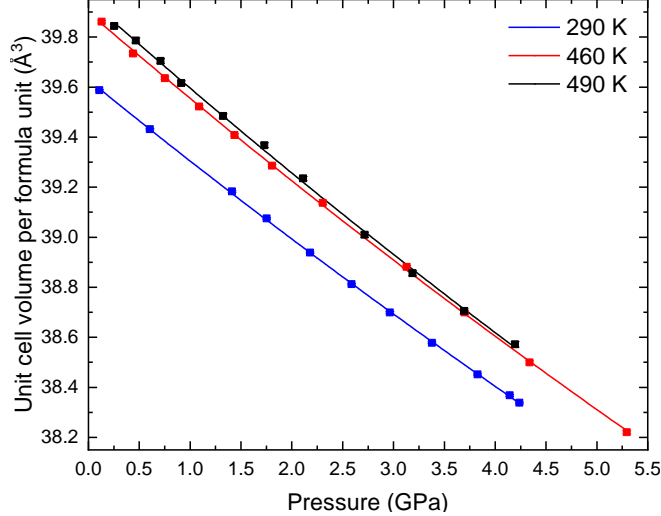


Figure 5: Variation in unit cell volume per formula unit for monoclinic $C2/m$ phase. Solid data points show experimental derived values and the solid line the determined 2nd-order Birch-Murnaghan equation of state. Full lattice parameters are found in SI Tables S3-5. Where error bars are not visible it is because they are smaller than the data points.

structure with positive thermal expansion. B decreases with increasing temperature, meaning that compressibility increases with temperature. At 290 K, B is 119.6(5) GPa. This is comparable with a similar JT-distorted material with edge-sharing octahedra, CuMnO_2 , which has bulk modulus 116(2) GPa.¹⁶ It is, however, substantially less than the reported bulk modulus for ZnMn_2O_4 of 197(5) GPa,¹⁴ and although there are several different reported values for Mn_3O_4 depending on phase and morphology,¹¹⁻¹³ all are higher than what we report for NaNiO_2 . LaMnO_3 is not entirely comparable owing to the LaO_{12} units and corner-sharing octahedra, but for reference it has a reported bulk modulus of 108(2) GPa.³

The directions of the principal axes of compression are determined using PASCAL⁵² [SI Figure S13]. These are the axes in which compression occurs linearly with pressure, and do not necessarily align with the crystallographic axes in crystalline materials. The principal axis directions projected onto the ab -plane do not change between the monoclinic and rhombohedral phases. However, the inter-layer direction is a principal axis for the rhombohedral phase, but not for the monoclinic phase where two principal axes are at an angle to the inter-layer direction [Fig. 1]. Interestingly, the axis of JT elongation does not correspond

to any of the principal axes [SI Table S11]. There is some temperature dependence in the principal axis directions, likely owing to variation in the lattice parameters with temperature [SI Tables. S3-S5]. The compressibilities of NaNiO_2 in each of the principal axes is consistent with variation in lattice parameters [SI Table S11].

We now consider pressure-dependence of the bond length distortion index and effective coordination [SI Figure S8; Tables S8-10]. As in the ambient pressure measurements the bond length distortions are significantly larger in the NiO_6 compared to the NaO_6 octahedra, with the most significant variation being the increase in effective coordination (5.387(10) at 0.107(8) GPa to 5.504(13) at 4.24(5) GPa at 290 K) and decrease in bond length distortion index (from 0.0512(5) to 0.0458(7) in the same pressure range at 290 K) of the NiO_6 octahedra in the monoclinic phase on application of pressure. NaO_6 octahedra exhibit far smaller changes in bond length distortion index and effective coordination, with the overall behaviour not seeming to exhibit a consistent change with pressure; effective coordination remains between 5.98 and 5.99 throughout the 290 K isotherm.

The differing behaviour of bond length distortion index between NiO_6 and NaO_6 octahedra is likely attributable to the fact that NiO_6 is JT-active and NaO_6 is not, and suggests that pressure is decreasing the magnitude of JT distortion. We investigate this by considering the direct manifestation of the JT effect in NaNiO_2 . The Ni-O bond lengths of both the monoclinic and rhombohedral phases as a function of pressure are shown in Figure 6. The short Ni-O bonds are less sensitive to the effect of pressure than the long Ni-O bonds, indicating that the difference between long and short Ni-O bond lengths is decreasing with pressure. We also observe that the average monoclinic bond length is consistently larger than the rhombohedral bond length at 490 K [SI Figure S9]. In the NaO_6 octahedra, SI Figure S5, there is an approximately linear variation of the Na-O bond lengths with pressure. We conclude that anisotropy of the Ni-O bond compression is a consequence of the JT distortion in NiO_6 octahedra.

The observed decrease in difference between long and short Ni-O bonds with pressure

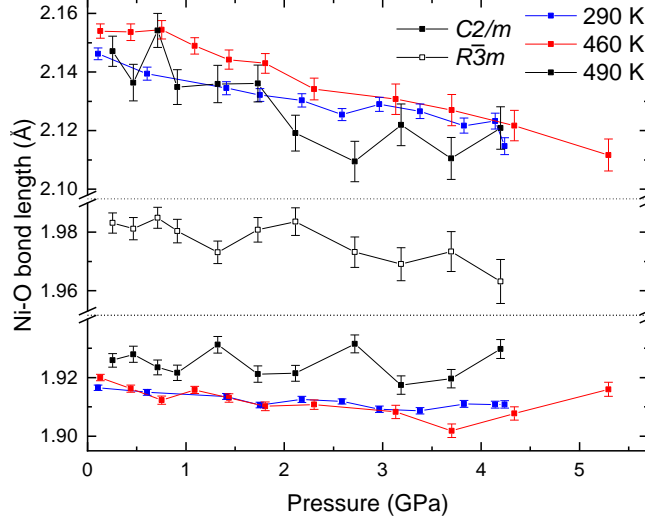


Figure 6: Ni-O bond lengths, as a function of pressure, and associated error of monoclinic NaNiO_2 at 290 K, 460 K, and 490 K, with the JT-inactive rhombohedral phase bond lengths shown for 490 K. Lines are a guide for the eye.

is also reported for other materials containing a JT distortion, such as LaMnO_3 ,³ KCuF_3 ,⁴ and CuAs_2O_4 .⁵ This is equivalent to the observed tendency with pressure of NiO_6 octahedra bond length distortion index and effective coordination towards their symmetry-constrained values of 0 and 6, respectively. It indicates that the symmetry of JT-distorted octahedra increases with application of pressure in monoclinic NaNiO_2 , consistent with prior reports.³⁻⁷

A previous study on LaMnO_3 attempted to extrapolate a linear fit to the pressure-dependence of JT-distorted bond length, and estimated a critical pressure of ~ 18 GPa.³ Such an extrapolation could be performed for NaNiO_2 yielding a critical pressure of ~ 50 GPa, converging at a Ni-O bond length of 1.85 \AA at 290 K. However, this value is unlikely to be representative of the true critical pressure of the JT distortion in NaNiO_2 . A later study on LaMnO_3 found that the JT distortion was suppressed at a lower pressure of around ~ 12 GPa, suggesting such extrapolation does not yield accurate predictions. Further, studies of other JT-distorted materials such as $[(\text{CH}_3)_2\text{NH}_2][\text{Cu}(\text{HCOO})_3]$ ⁶ and CuMnO_2 ¹⁶ have found that this pressure-dependence of JT-disproportionated bond length exists only up to a certain pressure, beyond which there is a change in behaviour which renders such extrapolation of low-pressure behaviour meaningless.

We earlier defined the bond angles $\theta_{\text{short-short}}^M$ and $\theta_{\text{long-short}}^M$ ($M=\text{Na},\text{Ni}$) for monoclinic NaNiO_2 , and the associated Δ values which reduce the number of parameters needed to describe the behaviour. We plot these Δ values in Figure 7 for the 290 K isotherm. These plots show that throughout the studied pressure range, the degree of angular distortion is far greater for NaO_6 than NiO_6 , as was the case at ambient pressure [Table 1]. We can also see that with application of pressure, Δ is decreasing in value; this indicates increasing symmetry towards the 90° degree bond angle for a perfect octahedron, analogous to the increasing symmetry with pressure we see with bond length distortion index.

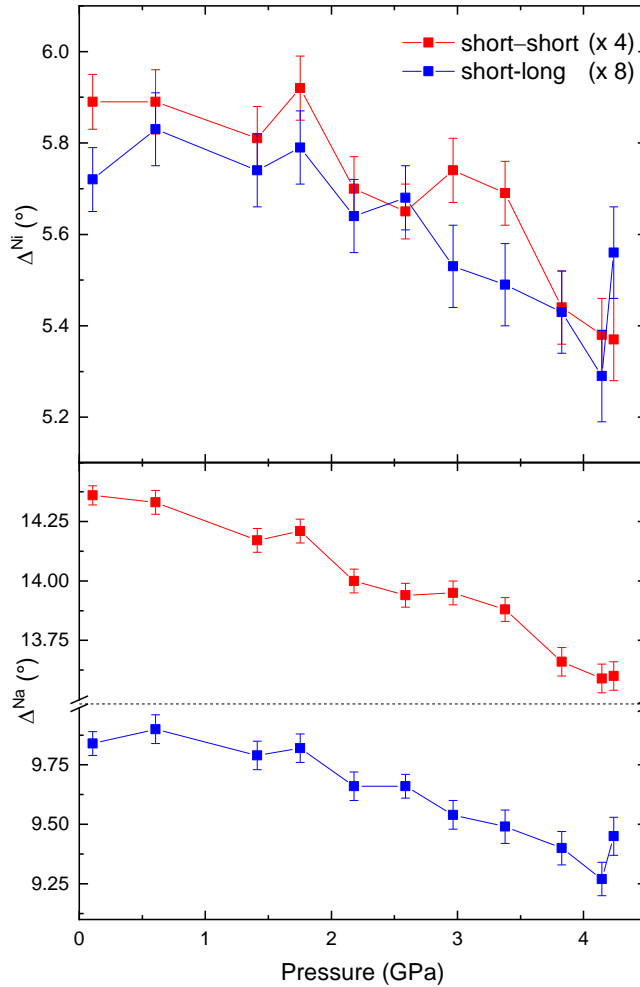


Figure 7: Values of Δ for NiO_6 and NaO_6 octahedra as a function of pressure at 290 K, representing the magnitude of angular distortion as nearest-neighbour bond angles take the value $90^\circ \pm \Delta$. The two different Δ values in monoclinic NaNiO_2 are between two short bonds (red) and between a short and long bond (blue), where bonds are short or long due to the JT distortion. Lines are a guide for the eye.

The pressure dependence of the NaO_6 and NiO_6 octahedral volume in NaNiO_2 [SI Figure S7] show that the changes in volume displays different pressure-dependence for NiO_6 octahedra and NaO_6 octahedra, as compared with the unit cell. NaO_6 octahedra have higher relative compressibility than the entire unit cell, and NiO_6 octahedra are much more resistant to compression. It has been shown that for perovskites with AO_{12} and BO_6 polyhedra the parameters M_A and M_B can be used to predict the relative compressibility of the polyhedra via $\beta_B/\beta_A = M_A/M_B$, in which $\beta_i = -\frac{1}{R_i} \frac{dR_i}{dP}$ is the bond compressibility, R_i is the distance between the central cation and the i th O anion, and M_i is a bond-valence parameter defined in SI.⁵⁴ We apply this model to NaNiO_2 and find that $M_{\text{Ni}} > M_{\text{Na}}$ throughout the 290 K isotherm [SI Figure S12]. Accounting for the different values of R_i , this indicates that $\frac{dR_{\text{Na-O}}}{dP} > \frac{dR_{\text{Ni-O}}}{dP}$, which is consistent with our observation that NaO_6 octahedra are more compressible than NiO_6 octahedra. This may be due to differences in electronic configuration for closed-shell Na^+ and open-shell Ni^{3+} , or Na^+ being a much larger ion than Ni^{3+} .

We now consider a related model proposed by Angel *et al.*, again in the context of perovskites,⁵⁵ whereby a transition temperature T_c associated with an octahedral phase transition will exhibit $dT_c/dP < 0$ if octahedra are more compressible than the extra-framework cation sites (analogous to the NaO_6 octahedra in NaNiO_2), and $dT_c/dP > 0$ if octahedra are less compressible. Our structural analysis shows the enhanced compressibility of NaO_6 octahedra when compared to NiO_6 , and so this model predicts the observed increase in T_{JT} with pressure. It is worth noting that there are more degrees of freedom in the layered NaNiO_2 structure so the relationships between distortions in NiO_6 and NaO_6 may not be so strongly coupled as in the perovskites. However, the basic hypothesis of the model in Angel *et al.* appears to be applicable to NaNiO_2 .

Along the 490 K isotherm, both monoclinic and rhombohedral NaNiO_2 were observed in coexistence. The fraction of NaNiO_2 in the low-temperature, JT-distorted monoclinic phase is shown in Figure 8. The fraction remains approximately stagnant to ~ 2 GPa, beyond which it consistently increases with increasing pressure. In the range where it is increasing,

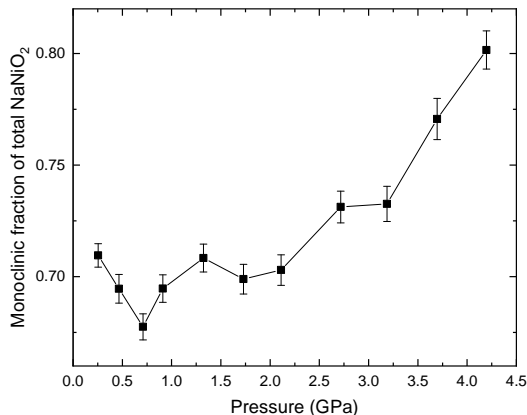


Figure 8: The fraction of NaNiO_2 which is in the monoclinic phase at 490 K, as a function of pressure.

the monoclinic fraction at 490 K increases from 67.8(6)% at 0.71(2) GPa to 80.2(9)% at 4.20(6) GPa. This indicates that T_{JT} increases with increasing pressure beyond ~ 2 GPa, consistent with our prediction based on octahedral compressibility.

To explore the P-T dependence of the transition, the sample was heated at 5.29(8) GPa from 460 K to 490 K after measuring the variable-pressure 460 K isotherm. At ambient pressure, this would result in a mixed monoclinic/rhombohedral phase. However, at the resulting high pressure of 5.46(9) GPa, we did not observe emergence of any rhombohedral peaks in the diffraction pattern. Subsequent reduction in pressure to 0.342(13) GPa at the same temperature, 490 K, did yield emergence of rhombohedral peaks [Figure S4], further supporting our interpretation that T_{JT} is increasing with pressure.

4 Discussion

The results of our P - T study on NaNiO_2 are summarised in a phase diagram, Figure 9. To our knowledge, this is the first study on the effect of pressure on the JT transition temperature in a material containing edge-sharing MO_6 octahedra, and the first variable-pressure study on a JT-active edge-sharing nickelate. Comparison between the results of this

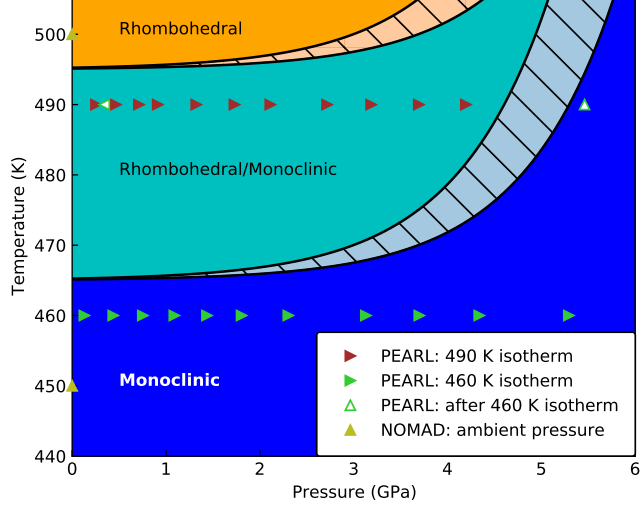


Figure 9: Tentative phase diagram showing the structure of NaNiO_2 as a function of pressure and temperature. Triangles denote diffraction measurements and point left/right if P was decreasing/increasing or up/down if T was increasing or decreasing. The precise boundaries of the three regions are estimates based on available data, with the results in Refs.^{31,46} used to estimate the broadness of the transition.

study and previous works must therefore rely on the work done on non-nickelate materials.

Like the perovskite materials LaMnO_3 ^{3,8} and KCuF_3 ,⁴ NaNiO_2 exhibits far greater compressibility in the JT-elongated O-Ni-O axis than the JT-compressed O-Ni-O axes, with the JT distortion in both NaNiO_2 and the previously-discussed perovskites decreasing in magnitude with pressure. The consistent behaviour with other JT-active materials is also clear evidence that the charge disproportionation model proposed for LiNiO_2 ^{26–28} and some Ni^{3+} -containing perovskites²¹ is not applicable to NaNiO_2 .

A novel behaviour we observe in NaNiO_2 is that T_{JT} increases with application of pressure NaNiO_2 . For comparison, in LaMnO_3 the JT distortion is suppressed at ~ 12 GPa, indicating that T_{JT} is reduced to room temperature from ~ 750 K by 12 GPa.² This mechanism seems unlikely in NaNiO_2 due to the increasing T_{JT} with pressure, although we cannot exclude the possibility that a reversal above our maximum measured pressure may result in a decrease in T_{JT} . Additionally, there is a trend observed in this, and other,^{3–7} works, that the magnitude of distortion due to the JT effect decreases with pressure. This could be interpreted as meaning that there is some pressure where the distortion is entirely suppressed and the

NiO₆ octahedra achieve a bond length distortion index of zero, consistent with absence of an ordered JT distortion. However, this is at odds with recent reports^{6,16} which show that at some pressure the long and short bonds in JT-distorted octahedra eventually stabilise at different lengths. It is therefore not clear how exactly the JT distortion is suppressed in NaNiO₂ with high pressure, and further investigation is needed to elucidate this.

We should once again note that the conductivity behaviour of the high-temperature phase of NaNiO₂ also remains unexplored. There is significant reduction in resistivity with JT suppression in LaMnO₃,¹⁰ and there is a possibility for similar behaviour in high-temperature rhombohedral NaNiO₂. Density Functional Theory calculations on rhombohedral, JT-free LiNiO₂ (which is isostructural with the high-temperature phase of NaNiO₂) have suggested metallic behaviour.⁵⁶ On a similar note, a broad first-order transition between two structures with a group-subgroup relationship in SrCrO₃⁵⁷ featured coexistence of electronic phases. If the high-temperature phase of NaNiO₂ were indeed metallic, this metallic behaviour could explain why $dT_{JT}/dP > 0$ in this material, as application of pressure may result in narrowing of Ni(3*d*)-O(2*p*) bands, pushing the metal-to-insulator phase transition to higher and higher temperatures, and electronic phase coexistence could provide an explanation for the very broad nature of the transition.

5 Conclusion

The key finding of this study is that in NaNiO₂, T_{JT} increases slightly with application of pressure while JT-distorted NiO₆ octahedra become more symmetric, as demonstrated by the pressure-dependence of two distortion metrics (effective coordination and bond length distortion index). While the latter is a well-documented property of JT-distorted materials, the former is in contrast to the JT distortion in LaMnO₃.² NaNiO₂ is more resistant to pressure than other similar materials, having a higher bulk modulus ($B = 119.6(5)$ GPa at 290 K) than similar perovskites,^{3,4} Prussian Blue analogues,⁷ and layered honeycomb structures,⁵⁰

although its bulk modulus is very similar to JT-distorted edge-sharing CuMnO_2 ,¹⁶ and is less than Mn_3O_4 ,^{11–13} NiO ,⁵⁸ and ZnMn_2O_4 .¹⁴ NaNiO_2 also displays a much smaller magnitude of $\frac{dT_{\text{JT}}}{dP}$ than LaMnO_3 , with LaMnO_3 shifting T_{JT} from ~ 750 K at ambient pressure to room temperature in 12 GPa^2 compared with a very small shift from ~ 480 K at ambient pressure in NaNiO_2 .

Further variable-pressure diffraction measurements, at several temperatures and to higher pressures, are needed to fully understand the process of suppressing the JT distortion in NaNiO_2 . Variable-pressure Raman spectroscopy measurements on NaNiO_2 could also be useful and may help identify phase transitions at higher pressures.

Additionally, future investigations are needed to investigate whether other JT-distorted materials exhibit a $dT_{\text{JT}}/dP > 0$ pressure dependence, for example a study building on previous work on CuMnO_2 ¹⁶ by measuring at multiple isotherms.

Data availability: The variable-pressure neutron diffraction data from the PEARL instrument at ISIS is available at doi:10.5286/ISIS.E.RB2000219.⁵⁹ All other data can be found at doi:10.17863/CAM.81605.⁶⁰

Acknowledgements

This work was supported by the Faraday Institution grant number FIRG017. LNC acknowledges a scholarship EP/R513180/1 to pursue doctoral research from the UK Engineering and Physical Sciences Research Council (EPSRC). Experiments at the ISIS Neutron and Muon Source were supported by a beamtime allocation RB2000219 from the Science and Technology Facilities Council of the United Kingdom. A portion of this research used resources at the Spallation Neutron Source, a DOE Office of Science User Facility operated by the Oak Ridge National Laboratory of the United States of America, with data collection performed by Joerg C Neufeind and Jue Liu (ORNL). Figure 1 was generated using CrystalMaker[®]: a crystal and molecular structures program from CrystalMaker Software Ltd, Oxford, UK.

Heather Greer assisted with the SEM images in Supplementary Information. We also thank others whose ideas and comments were useful: Joshua D Bocarsly, Farheen N Sayed, Andrew G Seel, Siddharth S Saxena, Euan N Bassey, Nicola D Kelly, Venkateswarlu Daramalla, Chloe S Coates, Camilla Tacconis, and Debasis Nayak.

Supplementary Information

The Supporting Information is available free of charge at ————. Additional neutron diffraction data and refinement details. SEM images. Tabulated diffraction data and distortion parameters. Transformation matrices.

References

- (1) Bhadram, V.; Joseph, B.; Delmonte, D.; Gilioli, E.; Baptiste, B.; Godec, Y. L.; Lobo, R.; Gauzzi, A. Reentrant phase transition and suppression of Jahn-Teller distortion in the quadruple perovskite structure under high pressure. *arXiv preprint arXiv:2102.09998* **2021**,
- (2) Zhou, J.-S.; Uwatoko, Y.; Matsubayashi, K.; Goodenough, J. Breakdown of magnetic order in Mott insulators with frustrated superexchange interaction. *Phys. Rev. B* **2008**, *78*, 220402.
- (3) Loa, I.; Adler, P.; Grzechnik, A.; Syassen, K.; Schwarz, U.; Hanfland, M.; Rozenberg, G. K.; Gorodetsky, P.; Pasternak, M. Pressure-induced quenching of the Jahn-Teller distortion and insulator-to-metal transition in LaMnO₃. *Phys. Rev. Lett.* **2001**, *87*, 125501.
- (4) Zhou, J.-S.; Alonso, J.; Han, J.; Fernández-Díaz, M.; Cheng, J.-G.; Goodenough, J. Jahn-Teller distortion in perovskite KCuF₃ under high pressure. *Journal of Fluorine Chemistry* **2011**, *132*, 1117–1121.

- (5) Caslin, K.; Kremer, R.; Razavi, F.; Hanfland, M.; Syassen, K.; Gordon, E.; Whangbo, M.-H. Competing Jahn-Teller distortions and hydrostatic pressure effects in the quasi-one-dimensional quantum ferromagnet CuAs_2O_4 . *Phys. Rev. B* **2016**, *93*, 022301.
- (6) Collings, I. E.; Bykov, M.; Bykova, E.; Hanfland, M.; van Smaalen, S.; Dubrovinsky, L.; Dubrovinskaia, N. Disorder–order transitions in the perovskite metal–organic frameworks $[(\text{CH}_3)_2\text{NH}_2][\text{M}(\text{HCOO})_3]$ at high pressure. *CrystEngComm* **2018**, *20*, 3512–3521.
- (7) Boström, H. L.; Collings, I. E.; Cairns, A. B.; Romao, C. P.; Goodwin, A. L. High-pressure behaviour of Prussian blue analogues: interplay of hydration, Jahn-Teller distortions and vacancies. *Dalton Transactions* **2019**, *48*, 1647–1655.
- (8) Pinsard-Gaudart, L.; Rodriguez-Carvajal, J.; Daoud-Aladine, A.; Goncharenko, I.; Medarde, M.; Smith, R.; Revcolevschi, A. Stability of the Jahn-Teller effect and magnetic study of LaMnO_3 under pressure. *Phys. Rev. B* **2001**, *64*, 064426.
- (9) Rodriguez-Carvajal, J.; Hennion, M.; Moussa, F.; Moudden, A.; Pinsard, L.; Revcolevschi, A. Neutron-diffraction study of the Jahn-Teller transition in stoichiometric LaMnO_3 . *Phys. Rev. B* **1998**, *57*, R3189.
- (10) Zhou, J.-S.; Goodenough, J. Paramagnetic phase in single-crystal LaMnO_3 . *Phys. Rev. B* **1999**, *60*, R15002.
- (11) Ovsyannikov, S. V.; Aslandukova, A. A.; Aslandukov, A.; Chariton, S.; Tsirlin, A. A.; Korobeynikov, I. V.; Morozova, N. V.; Fedotenko, T.; Khandarkhaeva, S.; Dubrovinsky, L. Structural stability and properties of marokite-type $\gamma\text{-Mn}_3\text{O}_4$. *Inorganic Chemistry* **2021**, *60*, 13440–13452.
- (12) Paris, E.; Ross II, C. R.; Olijnyk, H. Mn_3O_4 at high pressure: a diamond-anvil cell study and a structural modelling. *European Journal of Mineralogy* **1992**, 87–94.

- (13) Li, J.; Liu, B.; Dong, J.; Li, C.; Dong, Q.; Lin, T.; Liu, R.; Wang, P.; Shen, P.; Li, Q., et al. Size and morphology effects on the high pressure behaviors of Mn_3O_4 nanorods. *Nanoscale Advances* **2020**, *2*, 5841–5847.
- (14) Åsbrink, S.; Waśkowska, A.; Gerward, L.; Olsen, J. S.; Talik, E. High-pressure phase transition and properties of spinel ZnMn_2O_4 . *Phys. Rev. B* **1999**, *60*, 12651.
- (15) Choi, H.; Shim, J.; Min, B. Electronic structures and magnetic properties of spinel ZnMn_2O_4 under high pressure. *Phys. Rev. B* **2006**, *74*, 172103.
- (16) Lawler, K. V.; Smith, D.; Evans, S. R.; Dos Santos, A. M.; Molaison, J. J.; Bos, J.-W. G.; Mutka, H.; Henry, P. F.; Argyriou, D. N.; Salamat, A., et al. Decoupling Lattice and Magnetic Instabilities in Frustrated CuMnO_2 . *Inorganic Chemistry* **2021**, *60*, 6004–6015.
- (17) Medarde, M.; Mesot, J.; Rosenkranz, S.; Lacorre, P.; Marshall, W.; Klotz, S.; Loveday, J.; Hamel, G.; Hull, S.; Radaelli, P. Pressure-induced orthorhombic-rhombohedral phase transition in NdNiO_3 . *Physica B: Condensed Matter* **1997**, *234*, 15–17.
- (18) García-Muñoz, J.; Rodríguez-Carvajal, J.; Lacorre, P. Neutron-diffraction study of the magnetic ordering in the insulating regime of the perovskites $R\text{NiO}_3$ ($R = \text{Pr}$ and Nd). *Phys. Rev. B* **1994**, *50*, 978.
- (19) Mizokawa, T.; Khomskii, D.; Sawatzky, G. Spin and charge ordering in self-doped Mott insulators. *Phys. Rev. B* **2000**, *61*, 11263.
- (20) García-Muñoz, J.; Aranda, M.; Alonso, J.; Martínez-Lope, M. Structure and charge order in the antiferromagnetic band-insulating phase of NdNiO_3 . *Phys. Rev. B* **2009**, *79*, 134432.
- (21) Johnston, S.; Mukherjee, A.; Elfimov, I.; Berciu, M.; Sawatzky, G. A. Charge dispro-

- portionation without charge transfer in the rare-earth-element nickelates as a possible mechanism for the metal-insulator transition. *Phys. Rev. Lett.* **2014**, *112*, 106404.
- (22) Wawrzyńska, E.; Coldea, R.; Wheeler, E. M.; Mazin, I. I.; Johannes, M.; Sörgel, T.; Jansen, M.; Ibberson, R. M.; Radaelli, P. G. Orbital degeneracy removed by charge order in triangular antiferromagnet AgNiO_2 . *Phys. Rev. Lett.* **2007**, *99*, 157204.
- (23) Kang, J.-S.; Lee, S.; Kim, G.; Lee, H.; Song, H.; Shin, Y.; Han, S.; Hwang, C.; Jung, M.; Shin, H., et al. Valence and spin states in delafossite AgNiO_2 and the frustrated Jahn-Teller system ANiO_2 ($A = \text{Li, Na}$). *Phys. Rev. B* **2007**, *76*, 195122.
- (24) Rougier, A.; Delmas, C.; Chadwick, A. V. Non-cooperative Jahn-Teller effect in LiNiO_2 : an EXAFS study. *Solid State Communications* **1995**, *94*, 123–127.
- (25) Chung, J.-H.; Proffen, T.; Shamoto, S.; Ghorayeb, A.; Croguennec, L.; Tian, W.; Sales, B. C.; Jin, R.; Mandrus, D.; Egami, T. Local structure of LiNiO_2 studied by neutron diffraction. *Phys. Rev. B* **2005**, *71*, 064410.
- (26) Chen, H.; Freeman, C. L.; Harding, J. H. Charge disproportionation and Jahn-Teller distortion in LiNiO_2 and NaNiO_2 : A density functional theory study. *Phys. Rev. B* **2011**, *84*, 085108.
- (27) Foyevtsova, K.; Elfimov, I.; Rottler, J.; Sawatzky, G. A. LiNiO_2 as a high-entropy charge-and bond-disproportionated glass. *Phys. Rev. B* **2019**, *100*, 165104.
- (28) Green, R.; Wadati, H.; Regier, T.; Achkar, A.; McMahon, C.; Clancy, J.; Dabkowska, H.; Gaulin, B.; Sawatzky, G.; Hawthorn, D. Evidence for bond-disproportionation in LiNiO_2 from x-ray absorption spectroscopy. *arXiv preprint arXiv:2011.06441* **2020**,
- (29) Zhou, J.-S.; Goodenough, J. Chemical bonding and electronic structure of RNiO_3 ($R =$ rare earth). *Phys. Rev. B* **2004**, *69*, 153105.

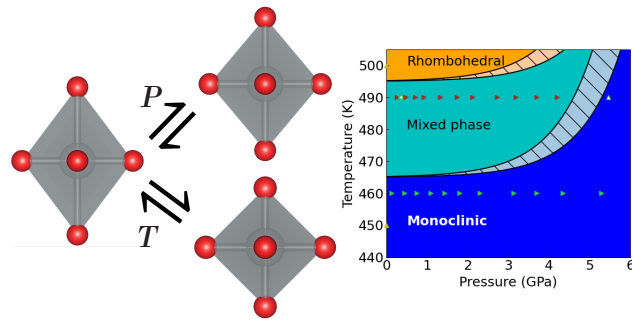
- (30) Dick, S.; Müller, M.; Preissinger, F.; Zeiske, T. The structure of monoclinic NaNiO_2 as determined by powder X-ray and neutron scattering. *Powder Diffraction* **1997**, *12*, 239–241.
- (31) Chappel, E.; Nunez-Regueiro, M.; Chouteau, G.; Isnard, O.; Darie, C. Study of the ferrodistorive orbital ordering in NaNiO_2 by neutron diffraction and submillimeter wave ESR. *The Euro. Phys. Journ. B-Cond. Matt. and Complex Systems* **2000**, *17*, 615–622.
- (32) Galakhov, V.; Kurmaev, E.; Neumann, M.; Kellerman, D.; Gorshkov, V., et al. Electronic structure of LiNiO_2 , LiFeO_2 and LiCrO_2 : X-ray photoelectron and X-ray emission study. *Solid State Communications* **1995**, *95*, 347–351.
- (33) Lewis, M.; Gaulin, B.; Filion, L.; Kallin, C.; Berlinsky, A.; Dabkowska, H.; Qiu, Y.; Copley, J. Ordering and spin waves in NaNiO_2 : A stacked quantum ferromagnet. *Phys. Rev. B* **2005**, *72*, 014408.
- (34) Baker, P.; Lancaster, T.; Blundell, S.; Brooks, M.; Hayes, W.; Prabhakaran, D.; Pratt, F. Thermodynamic and magnetic properties of the layered triangular magnet NaNiO_2 . *Phys. Rev. B* **2005**, *72*, 104414.
- (35) Darie, C.; Bordet, P.; De Brion, S.; Holzapfel, M.; Isnard, O.; Lecchi, A.; Lorenzo, J.; Suard, E. Magnetic structure of the spin-1/2 layer compound NaNiO_2 . *The Euro. Phys. Journ. B-Cond. Matt. and Complex Systems* **2005**, *43*, 159–162.
- (36) Vassilaras, P.; Ma, X.; Li, X.; Ceder, G. Electrochemical properties of monoclinic NaNiO_2 . *Journal of The Electrochem. Soc.* **2012**, *160*, A207.
- (37) Han, M. H.; Gonzalo, E.; Casas-Cabanas, M.; Rojo, T. Structural evolution and electrochemistry of monoclinic NaNiO_2 upon the first cycling process. *Journal of Power Sources* **2014**, *258*, 266–271.

- (38) Neufeind, J.; Feygenson, M.; Carruth, J.; Hoffmann, R.; Chipley, K. K. The nanoscale ordered materials diffractometer NOMAD at the spallation neutron source SNS. *Nuclear Instruments and Methods in Physics Research Section B: Beam Interactions with Materials and Atoms* **2012**, *287*, 68–75.
- (39) Bull, C. L.; Funnell, N. P.; Tucker, M. G.; Hull, S.; Francis, D. J.; Marshall, W. G. PEARL: the high pressure neutron powder diffractometer at ISIS. *High Pressure Research* **2016**, *36*, 493–511.
- (40) Fortes, A. D. RAL Technical Reports, RAL-TR-2019-002. **2019**,
- (41) Arnold, O.; Bilheux, J.-C.; Borreguero, J.; Buts, A.; Campbell, S. I.; Chapon, L.; Doucet, M.; Draper, N.; Leal, R. F.; Gigg, M., et al. Mantid—Data analysis and visualization package for neutron scattering and μ SR experiments. *Nuclear Instruments and Methods in Physics Research Section A: Accelerators, Spectrometers, Detectors and Associated Equipment* **2014**, *764*, 156–166.
- (42) Coelho, A. A. TOPAS and TOPAS-Academic: an optimization program integrating computer algebra and crystallographic objects written in C++. *Journal of Applied Crystallography* **2018**, *51*, 210–218.
- (43) Pawley, G. Unit-cell refinement from powder diffraction scans. *Journal of Applied Crystallography* **1981**, *14*, 357–361.
- (44) Rietveld, H. A profile refinement method for nuclear and magnetic structures. *Journal of Applied Crystallography* **1969**, *2*, 65–71.
- (45) Thompson, P.; Cox, D.; Hastings, J. Rietveld refinement of Debye-Scherrer synchrotron X-ray data from Al_2O_3 . *Journal of Applied Crystallography* **1987**, *20*, 79–83.
- (46) Sofin, M.; Jansen, M. New route of preparation and properties of NaNiO_2 . *Zeitschrift für Naturforschung B* **2005**, *60*, 701–704.

- (47) Hoppe, R. Effective coordination numbers (ECoN) and mean fictive ionic radii (MEFIR). *Zeitschrift für Kristallographie-Crystalline Materials* **1979**, *150*, 23–52.
- (48) Baur, W. The geometry of polyhedral distortions. Predictive relationships for the phosphate group. *Acta Crystallographica Section B: Structural Crystallography and Crystal Chemistry* **1974**, *30*, 1195–1215.
- (49) Kimber, S. A. Charge and orbital order in frustrated $\text{Pb}_3\text{Mn}_7\text{O}_{15}$. *Journal of Physics: Condensed Matter* **2012**, *24*, 186002.
- (50) Hermann, V.; Ebad-Allah, J.; Freund, F.; Pietsch, I.; Jesche, A.; Tsirlin, A. A.; Deisenhofer, J.; Hanfland, M.; Gegenwart, P.; Kuntscher, C. A. High-pressure versus isoelectronic doping effect on the honeycomb iridate Na_2IrO_3 . *Phys. Rev. B* **2017**, *96*, 195137.
- (51) Layek, S.; Mehlawat, K.; Levy, D.; Greenberg, E.; Pasternak, M.; Itié, J.-P.; Singh, Y.; Rozenberg, G. K. Electronic and structural properties of the honeycomb iridates $A_2\text{IrO}_3$ ($A = \text{Na}, \text{Li}$) at elevated pressures. *Phys. Rev. B* **2020**, *102*, 085156.
- (52) Cliffe, M. J.; Goodwin, A. L. PASCAL: a principal axis strain calculator for thermal expansion and compressibility determination. *Journal of Applied Crystallography* **2012**, *45*, 1321–1329.
- (53) Birch, F. Finite elastic strain of cubic crystals. *Physical Review* **1947**, *71*, 809.
- (54) Zhao, J.; Ross, N. L.; Angel, R. J. New view of the high-pressure behaviour of GdFeO_3 -type perovskites. *Acta Crystallographica Section B: Structural Science* **2004**, *60*, 263–271.
- (55) Angel, R. J.; Zhao, J.; Ross, N. L. General rules for predicting phase transitions in perovskites due to octahedral tilting. *Phys. Rev. Lett.* **2005**, *95*, 025503.
- (56) Chen, Z.; Zou, H.; Zhu, X.; Zou, J.; Cao, J. First-principle investigation of Jahn-Teller

- distortion and topological analysis of chemical bonds in LiNiO_2 . *Journal of Solid State Chemistry* **2011**, *184*, 1784–1790.
- (57) Ortega-San-Martin, L.; Williams, A. J.; Rodgers, J.; Attfield, J. P.; Heymann, G.; Huppertz, H. Microstrain sensitivity of orbital and electronic phase separation in SrCrO_3 . *Phys. Rev. Lett.* **2007**, *99*, 255701.
- (58) Eto, T.; Endo, S.; Imai, M.; Katayama, Y.; Kikegawa, T. Crystal structure of NiO under high pressure. *Phys. Rev. B* **2000**, *61*, 14984.
- (59) L. A. V. Nagle-Cocco, S. E. Dutton, and C. L. Bull. DOI:10.5286/ISIS.E.RB2000219. Behaviour of Jahn-Teller distorted NiO_6 octahedra in NaNiO_2 under pressure. 2021; <https://data.isis.stfc.ac.uk/doi/STUDY/113601628/>.
- (60) L. A. V. Nagle-Cocco, C. L. Bull, Christopher J. Ridley, S. E. Dutton. DOI:10.17863/CAM.81605. Data associated with "Pressure tuning the Jahn-Teller transition temperature in NaNiO_2 ". 2022; doi.org/10.17863/CAM.81605.

For Table of Contents Only



In this work, a variable-pressure neutron diffraction study on layered NaNiO_2 is presented, showing that pressure decreases the magnitude of distortion of Jahn-Teller-distorted Ni^{3+}O_6 octahedra while resulting in an increase in the Jahn-Teller suppression temperature, T_{JT} .